

Radio-quiet QSO environments - I. The correlation of QSOs and $b_J < 23$ galaxies.

Scott M. Croom^{*} and T. Shanks

Physics Department, University of Durham, South Road, Durham, DH1 3LE, England.

6 May 2021

ABSTRACT

In this paper we present results of an analysis of radio-quiet QSO environments. The aim is to determine the relation between QSOs, galaxies and the mass distribution as a function of redshift. We cross-correlate a sample of ~ 150 QSOs from optically and X-ray selected catalogues with faint, $b_J < 23$, galaxies. These data allow us to probe the galaxy clustering environment of QSOs out to $z \sim 1.0 - 1.5$. Far from giving a positive correlation, at $z < 1.5$ the QSO-galaxy cross-correlation function is marginally negative, with $\omega(\theta < 120'') = -0.027 \pm 0.020$. Colour information suggests that the anti-correlation is most significant between the QSOs and the red galaxy population.

We have constructed models to predict the QSO-galaxy cross-correlation, using the known form of the galaxy $N(z)$ at $b_J < 23$, and assuming a variety of clustering evolution rates. Cases in which QSOs exist in rich cluster environments are comfortably ruled out at more than 5σ and the results are more consistent with a ‘normal’ galaxy environment for radio-quiet QSOs. If the small anti-correlation is interpreted as an effect of gravitational lensing, this conclusion is not altered. In this case, the data are only $\sim 1\sigma$ below the low clustering amplitude models, while the high amplitude models are still comfortably rejected. We therefore conclude that these QSOs may not be much more highly biased than optically selected galaxies.

Key words: galaxies: clustering – galaxies: evolution - quasars: general

1 INTRODUCTION

Relating QSOs to the underlying mass distribution and to other mass tracers is a vital step in the process of using QSOs to measure large-scale structure in the Universe. In order to determine cosmological quantities, such as the density parameter Ω_0 , from the evolution of large-scale structure we are required to know the evolution of the *mass* distribution. Therefore, knowledge of the biasing of QSOs with respect to this mass distribution is of the utmost importance, and the relationship between galaxies and QSOs is an essential step in understanding this bias. The local environments of QSOs also give important clues to the physical processes which form these objects and control their evolution.

Direct imaging of the regions around QSOs is the most obvious way to investigate their environments. Yee & Green (1984) imaged $3' \times 3'$ fields centred on individual QSOs over a wide range in redshift, ($0.05 < z < 2.05$). They found significant numbers of excess galaxies (to a limiting magnitude of ~ 21 in the Gunn r band) associated with QSOs at $z < 0.5$. The luminosity distribution of the excess galaxies strongly

suggested that these QSOs are associated with galaxies at the distance implied by their cosmological redshift. Further investigations (Yee & Green 1987) showed that at $z \simeq 0.6$ some radio-loud QSOs were found in environments as rich as those of Abell class 1 clusters. Significant evolution was also detected from $z = 0.4$ to $z = 0.6$ in this radio-loud sample, with the QSO-galaxy covariance amplitude increasing by a factor of ~ 3 as redshift increases. An extension of this work (Ellingson et al. 1991) found that radio-quiet QSOs by contrast exist in significantly poorer environments than their radio-loud counter-parts. The results concerning radio-loud QSOs have been confirmed by several other independent studies (e.g. Hintzen et al. 1991) which found significant numbers of excess galaxies associated with QSOs out to $z \simeq 1.5$. However, observations of radio-quiet QSOs have found a range of results generally consistent with these objects existing in poorer environments, similar to that of an average galaxy. Smith, Boyle & Maddox (1995) find that the cross-correlation function between low redshift ($z \leq 0.3$) X-ray selected QSOs and $b_J < 20.5$ galaxies from the APM Galaxy Survey (Maddox et al. 1990) is consistent with the auto-correlation function of the APM Galaxy Survey, suggesting that this population of QSOs is unbiased with re-

^{*} S.M.Croom@durham.ac.uk

Table 1. Details of the AAT photographic plates used in our QSO-galaxy cross-correlation

Field Name	Plate No.	R.A. (B1950)	Dec. (B1950)	Emulsion/Filter
SGP2	J2801	00 49 39.4	-29 21 34	IIIaJ/GG385
SGP4	J1888	00 54 48.1	-27 54 45	IIIaJ/GG385
QSF3	J2719	03 40 18.0	-44 18 14	IIIaJ/GG385
F855	J1834	10 43 37.9	-00 04 48	IIIaJ/GG385
	R1835	10 43 37.9	-00 04 48	IIIaF/RG630
F864	J1836	13 41 14.0	-00 00 29	IIIaJ/GG385
	R1837	13 41 14.0	-00 00 29	IIIaF/RG630

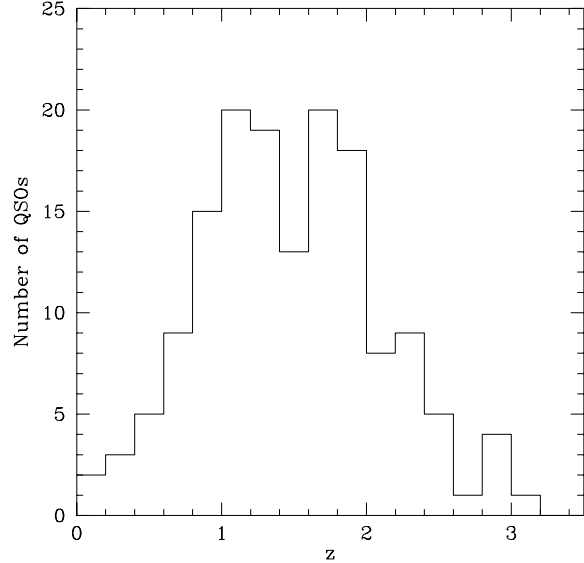
spect to galaxies. Extending this work, Smith (1998) finds that X-ray selected QSOs to $z = 0.7$ exist in poor environments. Boyle & Couch (1993) have found no excess galaxy population associated with radio-quiet QSOs at $z \sim 1$, while Hutchings, Crampton & Johnson (1995) find that a number (9 out of 14) of radio-quiet QSOs exist in compact groups of star forming galaxies at $z = 1.1$. Clearly there is a difference between radio-loud and radio-quiet QSOs, with radio-loud QSOs inhabiting richer environments. Radio-quiet QSOs appear to inhabit environments similar to those of normal galaxies, although the Hutchings et al. result is somewhat discrepant from this hypothesis. In this paper we will further investigate the problem of QSO environments with a large (~ 150) sample of optically and X-ray selected QSOs covering a wide range in redshift. The second paper in the series (Croom & Shanks 1998, in preparation) will use deeper imaging to constrain QSO environments at higher redshift.

In Section 2 we describe our data and the methods employed. We present our cross-correlation results in Section 3, and compare them to model predictions in Section 4. A discussion of our results and our conclusions are contained in Sections 5 and 6.

2 DATA AND METHODS

The faint galaxy samples were taken from deep AAT plates in five $40' \times 40'$ fields. Details of the plates are given in Table 1. Each field has a b_J plate and two fields also have r_F plates. The plates were scanned by the COSMOS measuring machine. Details of the analysis of the first 3 fields (SGP2, SGP4, QSF3), including star-galaxy separation and photometric calibration are given in Jones et al. (1991). Fields F855 and F864 (Roche et al. 1995; Roche 1994) were similarly analysed. The plate scale for all five fields is 15.2 arcsec/mm. The magnitude limit for the b_J plates is $\simeq 24$ mag and the completeness limit is $b_J = 23.5$. We use the galaxies to a limiting magnitude of $b_J = 23.0$, which is comfortably brighter than the completeness limit. At this magnitude the errors in the star-galaxy separation are $\sim 5\%$.

The QSOs in this analysis are from both optically and X-ray selected samples. Fields SGP2, SGP4 and QSF3 contain QSOs from the Durham/AAT UVX selected sample

**Figure 1.** The redshift distribution of all the QSOs, optically and X-ray selected, used in this analysis. The total number of QSOs is 152.

(Boyle et al. 1990), limited to $B = 21$ mag. The F855 and F864 fields contain QSOs from the deeper ESO/AAT colour selected sample (Boyle et al. 1991; Zitelli et al. 1992) with a limiting magnitude of $B = 22.5$. The X-ray selected QSOs were taken from optical follow-up of a deep *ROSAT* survey (Almaini 1996; Shanks et al. 1998). The QSOs are $> 4\sigma$ detections with the *ROSAT* Position Sensitive Proportional Counter (PSPC). Details of the QSO samples used are given in Table 2, and the redshift distribution of the combined sample of 152 QSOs is shown in Fig. 1. It should be noted that a large number of QSOs were selected independently using both optical and X-ray techniques. As pointed out in Section 1, radio-loud and radio-quiet QSOs appear to have different environments. We have therefore attempted to determine whether any of our optically and X-ray selected QSOs are, in fact, radio-loud. Using the NRAO VLA Sky Survey (NVSS) (Condon et al. 1998) at $\delta > -40^\circ$ and the Parkes-MIT-NRAO (PMN) Survey at $\delta < -40^\circ$ (Gregory et al. 1994) we find that none of our QSOs are within $30''$ of a radio source at the ~ 2.5 mJy level (NVSS) and ~ 25 mJy (PMN). This is somewhat surprising, as we expect $\sim 5\%$ of optically selected QSOs to be radio-loud.

The QSO coordinates (optical counterpart positions in the case of the X-ray selected objects) were transformed to the x,y system of the COSMOS scanned b_J plates using the Starlink ASTROM software; ~ 40 stars were used to produce the 6 coefficient transform. The RMS residuals for these transforms are shown in Table 2, all are less than $1''$. The five fields are plotted in Fig 2, showing all galaxies to $b_J = 23$ with the positions of the QSOs overlaid on top of this.

The cross-correlation was carried out in the standard manner, with the galaxy distribution being compared to a random distribution of points with the same angular selection function (that is avoiding holes) as the galaxies. The number density of randoms was 100 times the density of

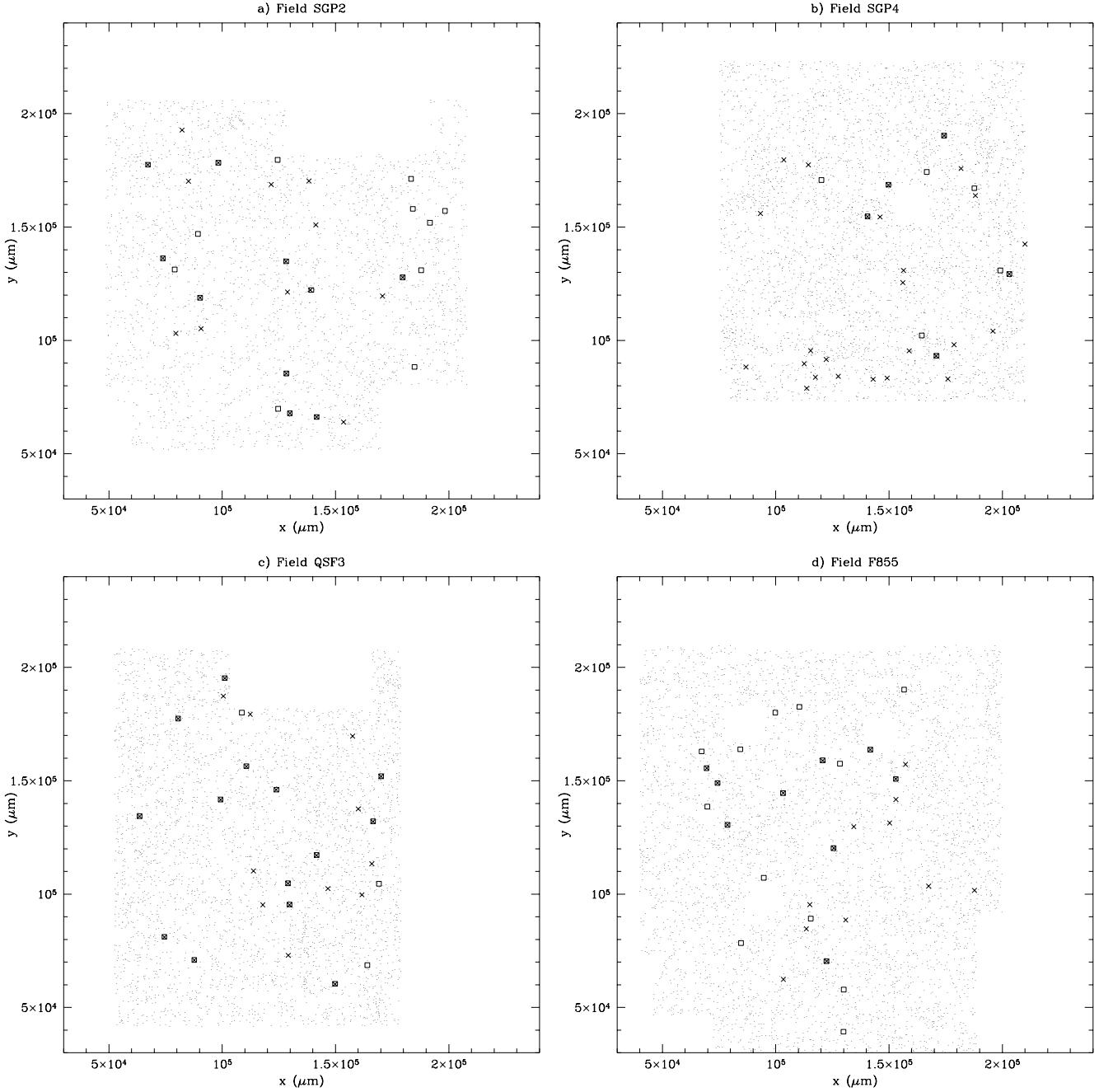


Figure 2. The x,y positions of galaxies to $b_J = 23$ from COSMOS scans of AAT photographic plates, together with the positions of the QSOs. a) Field SGP2, b) field SGP4, c) field QSF3, d) field F855, e) field F864. Open squares are the optically selected QSOs while crosses are the X-ray selected QSOs, The regions removed due to plate defects and bright stars can be seen. It should be noted that a number of QSOs are both optically and x-ray selected.

galaxies. The angular cross-correlation function, $\omega_{\text{qg}}(\theta)$, is defined as

$$\omega_{\text{qg}}(\theta) = \frac{N_{\text{qg}}(\theta)N_{\text{r}}}{N_{\text{qr}}(\theta)N_{\text{g}}} - 1, \quad (1)$$

where N_{r} is the total number of random points, N_{g} is the total number of galaxies, and N_{qg} and N_{qr} are the number of QSO-galaxy and QSO-random pairs with separation $\theta \pm \delta\theta/2$ respectively. This was calculated in concentric an-

nuli of width $30''$. The inner $5''$ is removed to avoid any confusion between very near companions and the QSOs themselves, and any QSOs which might have been classified as galaxies on the COSMOS scans. The errors shown in the figures below are Poisson errors:

$$\Delta\omega = \frac{\omega(\theta) + 1}{\sqrt{N_{\text{qg}}}}. \quad (2)$$

To test the Poisson error estimates we carry out two tests;

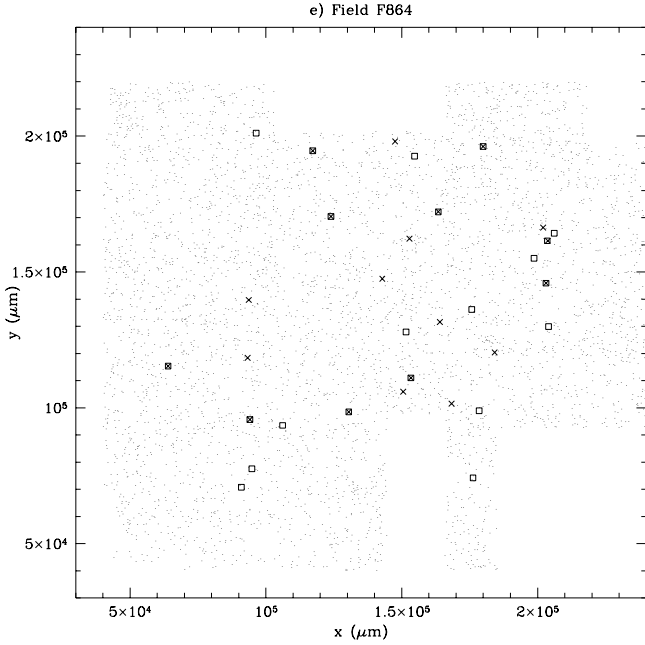


Figure 2. Cont.

Table 2. Details of the QSO samples used in this analysis. It should be noted that many QSOs were selected by both optical and X-ray methods.

Field Name	No. of Opt. QSOs	No. of X-ray QSOs	Total No. of QSOs	r.m.s. Ast. (")
SGP2	20	20	30	0.86
SGP4	10	27	33	0.43
QSF3	17	24	26	0.39
F855	21	19	31	0.26
F864	22	20	32	0.69

the first is to replace the QSOs with a random selection of galaxies and carry out a cross-correlation between these random galaxies and the rest of the galaxy sample. A variance is calculated from 100 realizations of this process. The second test calculates the cross-correlation between the QSOs and a bootstrap re-sampled galaxy distribution, again using 100 realizations to find a variance. For all QSOs with $z < 1.5$ the Poisson error on the amplitude within $120''$ is ± 0.020 (see Section 3 below). The error estimated from replacing QSOs with random galaxies is ± 0.026 while the bootstrap estimator gives ± 0.020 . The excess variance from the first test is due to the positive galaxy auto-correlation. The bootstrap method uses the QSO-galaxy cross-correlation which, as we show below, has no significant clustering signal.

The background density of galaxies is determined from each field separately which forces the integral of $\omega(\theta)$ to be zero at the largest scales studied. This is the well known ‘integral constraint’, which is simply due to the fact that there is still appreciable clustering of galaxies on the scale of our fields. In our case we do not know *a priori* that there

will be a significant signal on scales of $\sim 20'$, therefore an accurate estimate of the integral constraint is not possible. Given this, we can still determine a possible integral constraint correction in order to investigate its possible effect on our results. The angular correlation function determined in an area Ω is biased low by the amount

$$I = \frac{1}{\Omega^2} \int \int \omega(\theta_{12}) d\Omega_1 d\Omega_2. \quad (3)$$

We then assume the standard power-law for the cross-correlation function, $\omega(\theta) = A\theta^{-0.8}$. We find the following integral constraint for the five fields: 3.29A (SGP2), 3.42A (SGP4), 3.36A (QSF3), 3.04A (F855) and 2.89A (F864). The auto-correlation function amplitude for $b_J \sim 23$ galaxies is ~ 0.002 . If we were to assume that this value was a reasonable estimate of the QSO-galaxy cross-correlation then the integral constraint in our fields would be ~ 0.006 . We will demonstrate below that the addition of an integral constraint of this amplitude has no significant effect on our conclusions.

3 CROSS-CORRELATION RESULTS

We now present the results of the cross-correlation analysis between both the optically and X-ray selected QSOs and the galaxy catalogues. First, we look at the angular cross-correlation function for each field individually; these are shown in Fig. 3a-e while Fig. 3f shows a combination of all five fields. We show the results for all the known QSOs within each field (X-ray and optically selected QSOs combined). From these plots it is clear that there is a significant *anti-correlation* in the F855 and F864 fields while the SGP4 field is the only one which appears to show a positive correlation. The combined cross-correlation function therefore shows a small negative signal on small scales. Fig. 3 was derived using all the QSOs in each field (including the whole range of redshifts and both X-ray and optically selected objects). In order to look in detail at the source of the signal we calculate below a clustering amplitude for each individual QSO.

We calculate the individual cross-clustering amplitude for each QSO in a non-parametric fashion, simply using the integrated excess of galaxies out to a defined radius which we choose to be $120''$, giving $\omega(\theta < 120'')$ (still using an inner limit of $5''$). A radius of $120''$ is equivalent to $0.5 h^{-1}$ Mpc in proper co-ordinates at a redshift of $z \sim 1$ for an $\Omega_0 = 1$ flat Universe. We can relate this measure of clustering to a parametric clustering amplitude assuming the simple power-law form for the angular cross-correlation function,

$$\omega_{qg}(\theta) = A_{qg}\theta^{1-\gamma}. \quad (4)$$

The number of QSO-galaxy pairs between θ_1 and θ_2 is

$$N_{qg}(\theta_1 \leq \theta \leq \theta_2) = \frac{2N_g}{\theta_2^2 - \theta_1^2} \int_{\theta_1}^{\theta_2} \theta(1 + \omega_{qg}(\theta))d\theta, \quad (5)$$

where N_g is the number of galaxies. This can then be used to relate the non-parametric $\omega(\theta < 120'')$ to the clustering amplitude A_{qg} via Eq. 1 for $5'' \leq \theta \leq 120''$. We assume a power-law slope with $\gamma = 1.8$.

In Fig. 4 we show the clustering amplitudes for individual QSOs within $120''$ as a function of redshift for each field.

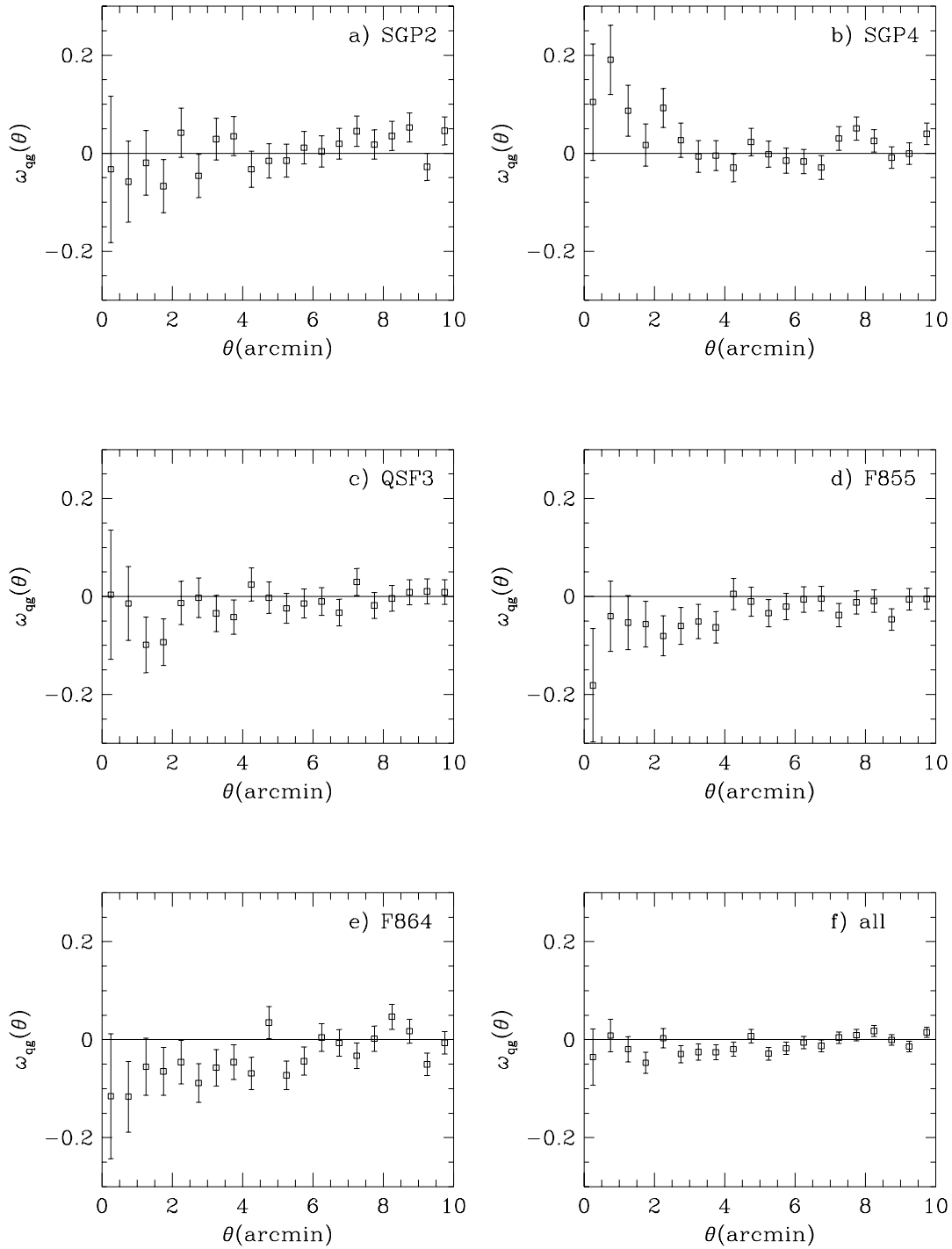


Figure 3. The QSO-galaxy angular cross-correlation function for each of the five AAT fields individually, including all QSOs. f) shows a pair weighted combination of all five fields.

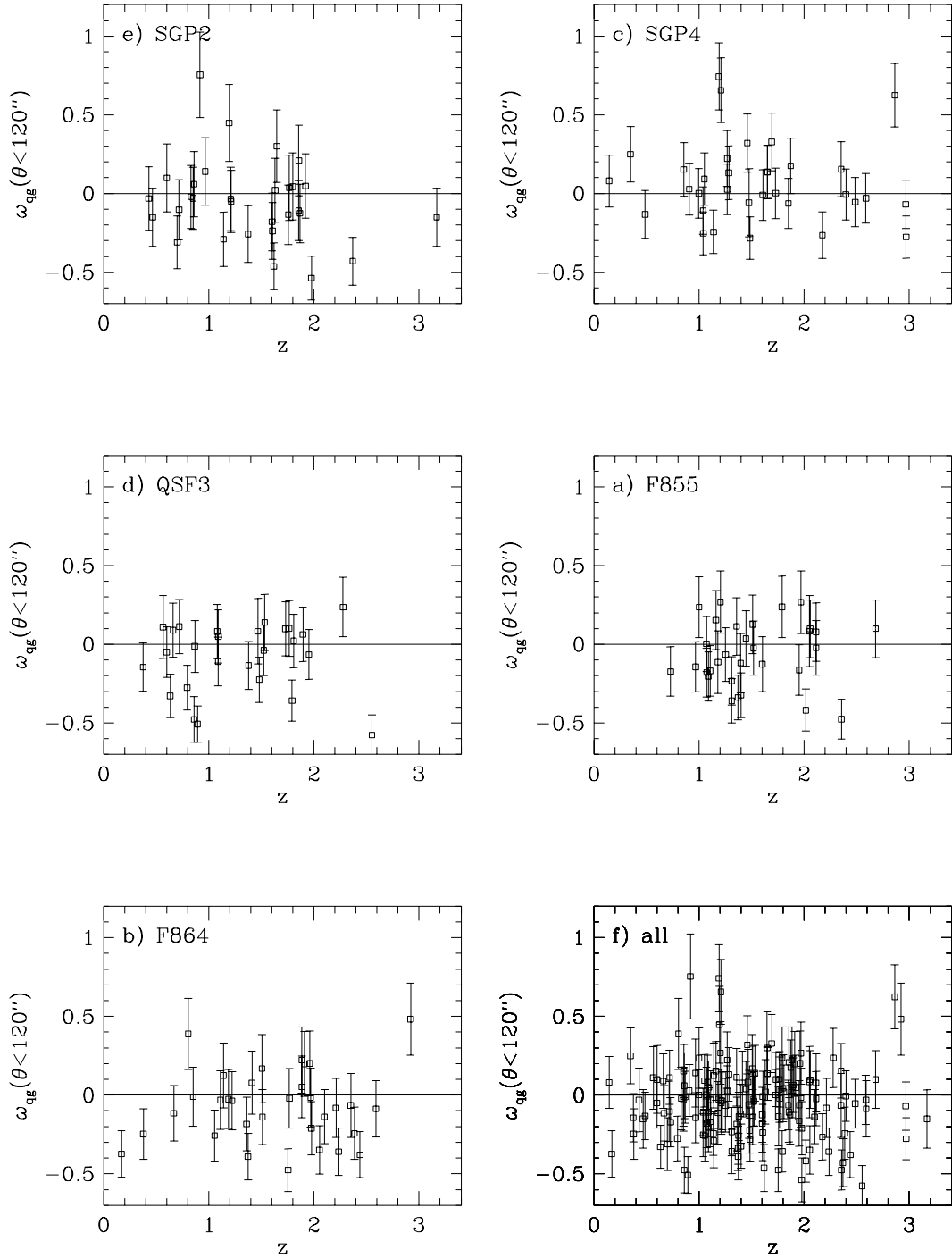


Figure 4. The QSO-galaxy clustering amplitude for individual QSOs in each AAT field (both optically and X-ray selected QSOs) as a function of redshift. f) shows all fields combined. Individual clustering amplitudes are measured within a radius of $120''$.

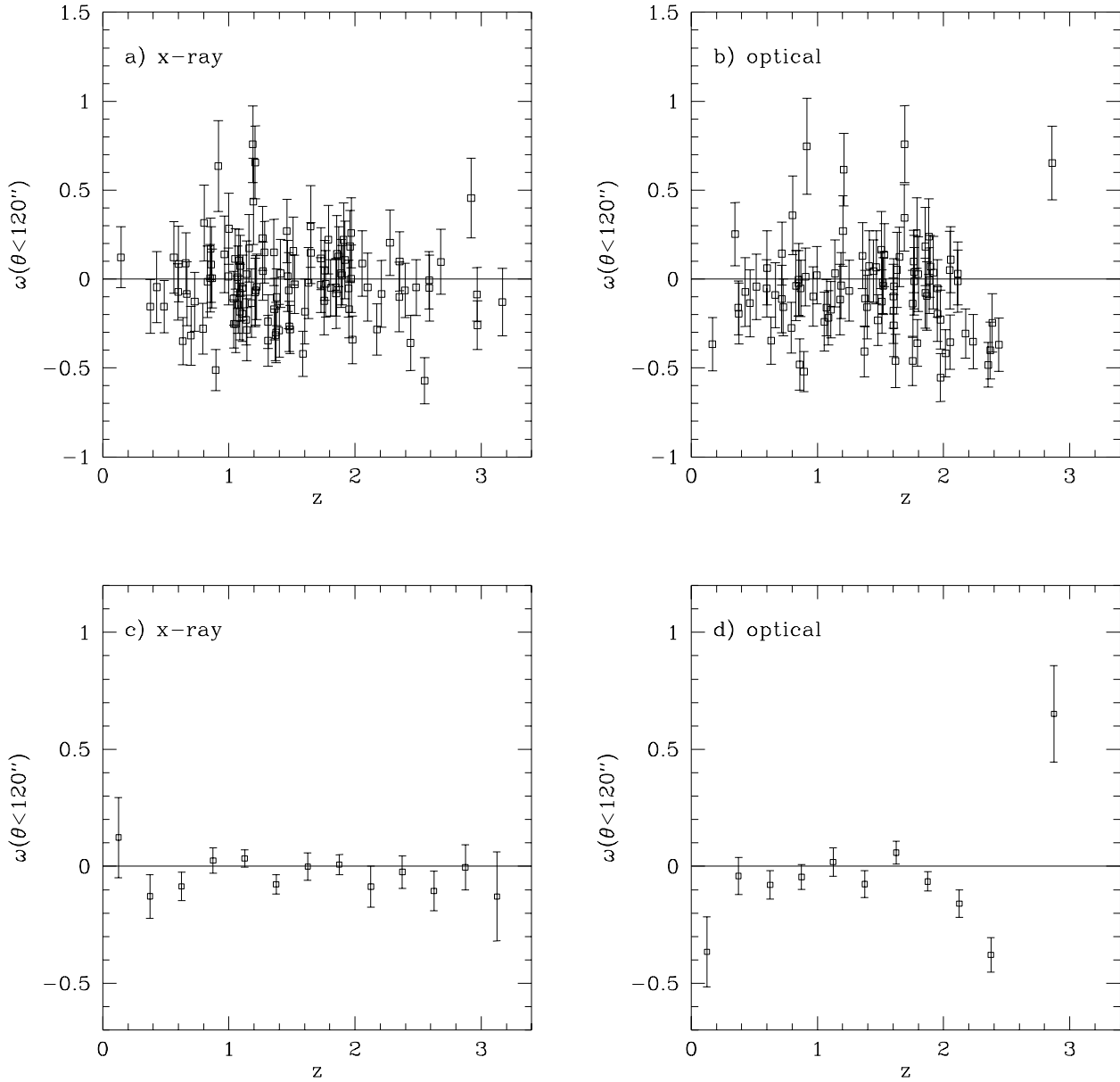


Figure 5. QSO-galaxy clustering amplitudes within $120''$ for QSOs as a function of redshift. a) individual X-ray selected QSOs and b) individual optically selected QSOs. c) and d) show the same data binned as a function of redshift with $\Delta z = 0.25$.

These show that the positive correlation in the SGP4 field is mainly due to three QSOs with strong positive signals. One of these is at $z = 2.861$ and has $\omega(\theta < 120'') = 0.62 \pm 0.20$ (equivalent to $A_{\text{qg}} = 0.025 \pm 0.008$). We do not expect to see any galaxies brighter than $b_J = 23$ at this redshift and hence this is either a chance alignment or the effect of gravitational lensing on the QSO. Examination of this object by eye confirms that there is a concentration of faint objects close to the QSO which could be a cluster of galaxies. The second of the three objects is only separated from the $z = 2.861$ QSO by $\sim 1'$. The third also shows a number of faint objects very

close to the QSO. By contrast, the negative signal in fields F855 and F864 is seen to be due to a large number of objects with $\omega(\theta < 120'') \sim -0.2$ to -0.5 . There is no measurable correlation between redshift and clustering amplitude (determined from a non-parametric rank-correlation test), with objects over the entire range in redshift contributing to the negative signal.

We should note that using galaxies from the AAT plates to the plate limit of $b_J \sim 24$ does not have any effect on the results presented here. The clustering amplitudes are not significantly altered, although obviously the Poisson errors

are somewhat reduced by the increased number of galaxies. Considering that at this magnitude limit the sample is incomplete and the star-galaxy separation is ill-defined, a limit of $b_J = 23$ affords a more robust and reliable result.

The clustering amplitudes for individual QSOs separated on the basis of their selection (X-ray or optical) are shown in Fig. 5. It should be noted that a large fraction of the QSOs were selected independently by both X-ray and optical techniques. Of course, the X-ray selected sample also has an implicit optical selection imposed on it due to the need to identify an optical counterpart to the X-ray source on which to carry out follow-up spectroscopy. Fig. 5 shows that almost all of the QSOs show zero or negative correlation amplitudes, while there are a small number of outlying objects with significant positive signal. The only difference between the X-ray and optically selected QSOs is a possible anti-correlation in the optical sample at high, $z > 1.8$, redshift. This can be seen more clearly if the results are combined in redshift intervals, as shown in Figs. 5c and d. Here we combine the galaxy counts around each QSO in $\Delta z = 0.25$ intervals. The X-ray selected sample (Fig. 5c) shows no significant signal or trend as a function of redshift. The optically selected sample (Fig. 5d) shows a significant anti-correlation at redshifts greater than $z \sim 1.8$, with the other significant points (in the first and last redshift bins) both due to individual QSOs. At low redshift, where any signal due to real associations would be expected, none is detected; at $z < 1.5$, $\omega(\theta < 120'') = -0.018 \pm 0.022$ for the X-ray selected sample and -0.051 ± 0.027 for the optical sample. For the combined sample of all QSOs with $z < 1.5$ we obtain $\omega(\theta < 120'') = -0.027 \pm 0.020$ (82 QSOs). In the next section these results are compared to the expected values for given clustering amplitudes and clustering evolution.

We have colour information in two fields, with F855 and F864 containing r_F plates. The colour distribution of the galaxies peaks at $b_J - r_F \simeq 1.25$ so we use this limit to define red and blue galaxy populations. Fig. 6 shows the results of this analysis, with Figs. 6a and 6b showing the angular correlation functions for all QSOs. The red galaxies appear to contribute more to the anti-correlation seen in the F855 and F864 fields. When we look at the clustering amplitudes of individual QSOs at $\theta < 120''$ we see no obvious trend (Figs. 6c, d), but binning these results as a function of redshift we see that the blue galaxies show no strong correlation or anti-correlation at any redshift, while the red galaxies appear to show generally negative correlations (similar to that seen in the correlation of all galaxies with the optically selected QSOs, Fig. 5d). At $z < 1.5$ the correlations for the red and blue populations are $\omega(\theta < 120'') = -0.093 \pm 0.043$ and -0.057 ± 0.048 respectively. Further dividing the sample into X-ray and optically selected QSOs we see no significant differences, this is mostly due to the increased errors from a smaller number of QSOs.

We therefore see tentative evidence for a difference in the cross-clustering properties of red and blue galaxies with QSOs. Any physical process which would cause this effect will be largely due to the fact that red and blue galaxies tend to inhabit different environments. Red galaxies are found in richer environments and are more strongly clustered than blue galaxies, which tend to inhabit the field rather than clusters. This hints at gravitational lensing as a mechanism for the anti-correlation. Below we make some estimates of

the expected QSO-galaxy cross-correlation and relate them to the results found here.

4 MODELLING QSO ENVIRONMENTS

4.1 Limber's equation

The angular cross-correlation function, $\omega_{ab}(\theta)$, between two populations, a and b , can be related to the spatial cross-correlation function $\xi_{ab}(r, z)$ by Limber's equation (Limber 1953; Peebles 1980) which can be written as

$$\omega_{ab}(\theta) = \frac{2 \int_0^\infty \int_0^\infty x^4 F^{-2} \phi_a(x) \phi_b(x) \xi_{ab}(r, z) dx du}{\int_0^\infty x^2 F^{-1} \phi_a(x) dx \int_0^\infty x^2 F^{-1} \phi_b(x) dx}, \quad (6)$$

under the assumption that the integral is dominated by objects at almost equal cosmic distance. The F term accounts for varying cosmological geometries and is given by

$$F = \left[1 - \left(\frac{H_0 a_0 x}{c} \right)^2 (\Omega_0 - 1) \right]^{1/2}. \quad (7)$$

We will assume a flat cosmology with $\Omega_0 = 1$, that is $F = 1$. The comoving distance to a point midway between a and b is given by x (assuming that the separation of a and b is small compared to x). The small angle approximation is also assumed so that the proper separation between a and b is

$$r = \frac{1}{1+z} \left(\frac{u^2}{F^2} + x^2 \theta^2 \right)^{1/2}, \quad u = x_b - x_a. \quad (8)$$

$\phi_a(x)$ and $\phi_b(x)$ are the selection functions for the two populations and satisfy

$$\int_0^\infty x^2 \phi(x) dx = \int_0^\infty N(z) dz, \quad (9)$$

where $N(z) dz$ is the number of objects per unit surface area in the redshift interval $[z, z + dz]$.

We parameterize the spatial cross-correlation function in the conventional power-law form:

$$\xi_{ab}(r, z) = \left(\frac{r}{r_0} \right)^{-\gamma} (1+z)^{-(3+\epsilon)}, \quad (10)$$

where r is the proper separation of two objects and r_0 is the correlation scale length at $z = 0$. Evolution is parameterized by ϵ , with various values of this parameter corresponding to the following cases: $\epsilon = 0$ is equivalent to constant clustering in proper coordinates, so called *stable clustering*; $\epsilon = \gamma - 3$ implies clustering which is constant in comoving coordinates; $\epsilon = \gamma - 1$ implies clustering which grows according to linear theory (for $\Omega_0 = 1$). We adopt the standard locally measured galaxy auto-correlation power-law slope of $\gamma = 1.8$. Although this is not necessarily correct at high redshift or in the case of QSO-galaxy cross-correlations, the measured QSO auto-correlation is consistent with this slope (Croom & Shanks 1996). We investigated the effect of altering the slope and found that a change in slope of ~ 0.2 does not significantly alter our conclusions.

The conversion from spatial to angular cross-correlation function is obviously strongly dependent on the radial selection functions, $\phi(x)$, of the two populations. For the QSOs we simply use the redshift distribution of the QSOs used in our analysis above (Section 3), that is, we integrate Limber's equation over all the QSOs in the sample. To model

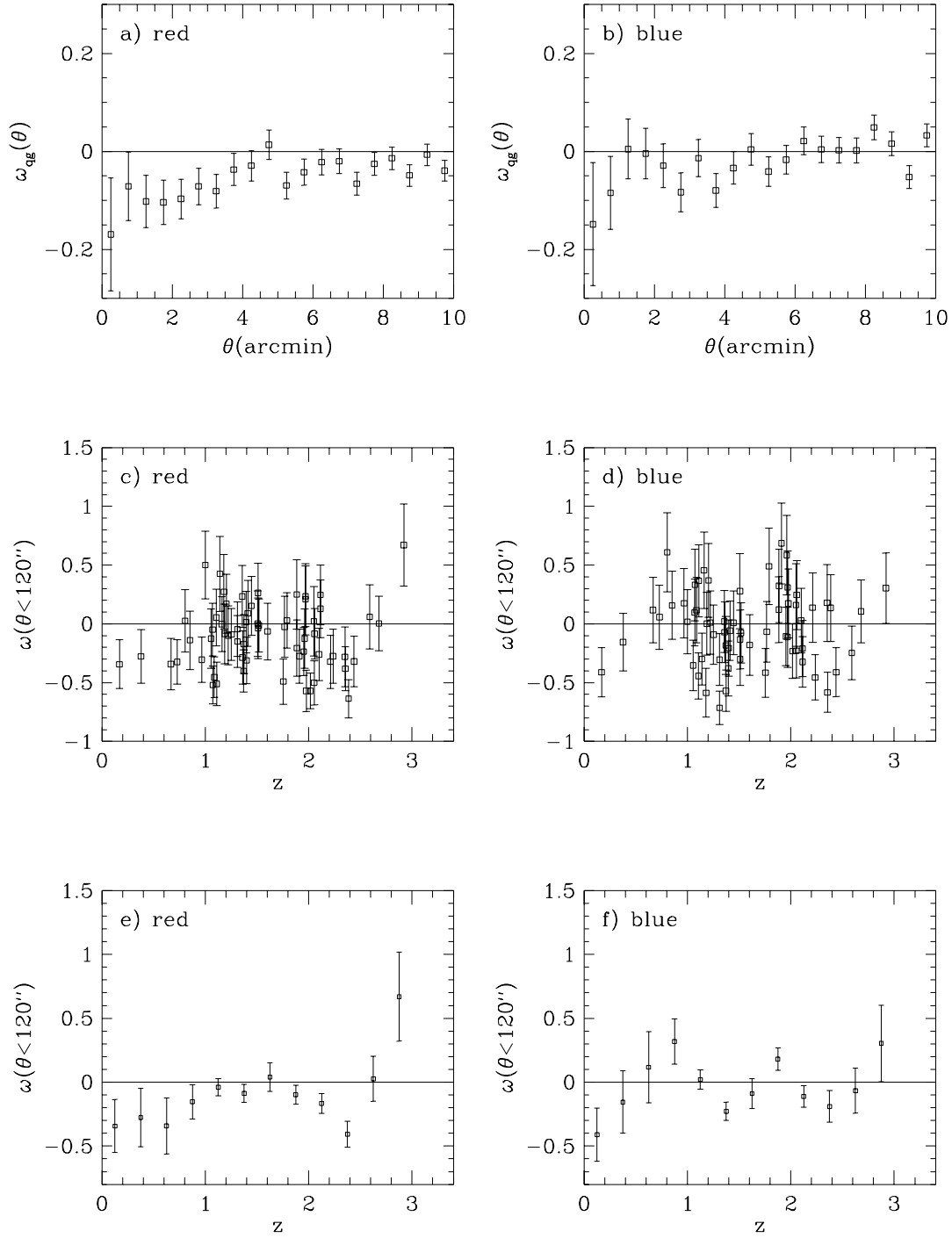


Figure 6. Results for the QSO cross-correlation with colour selected galaxies. The angular cross-correlation function for a) red and b) blue galaxies. The clustering amplitude within $120''$ for individual QSOs with c) red and d) blue galaxies as a function of redshift, and the redshift binned clustering amplitude for e) red and f) blue galaxies.

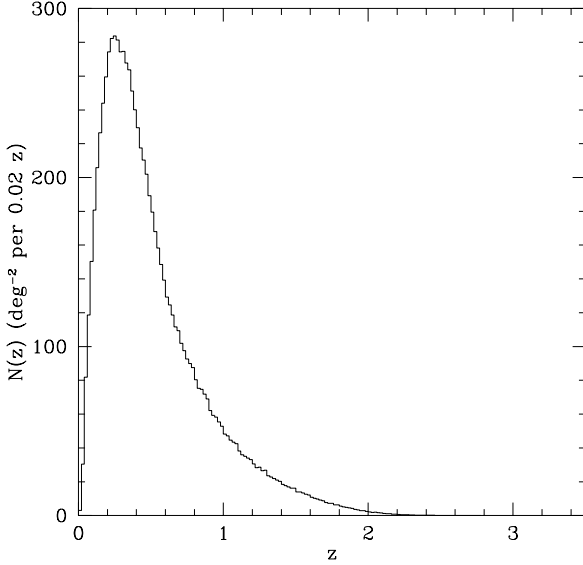


Figure 7. The model redshift distribution from Metcalfe et al. (1996) for a limiting magnitude of $b_J = 23$.

the galaxy selection function, we use the $N(z)$ derived from the galaxy evolution model of Metcalfe et al. (1996) which is consistent with the redshift distribution of galaxies in the deep Keck Telescope galaxy redshift survey to $B = 24$ (Cowie et al. 1995). These models contain an exponential rise in star formation with look-back time and use the evolutionary tracks of Bruzual & Charlot (1993). The $N(z)$ distribution from this model is shown in Fig. 7. It should be noted that the luminosity evolution produces a considerable high redshift tail to the distribution, as found in the sample of Cowie et al., where significant numbers of galaxies were found above $z = 1$.

Therefore, the only free parameters we have are the clustering correlation length r_0 and the evolutionary parameter ϵ , which we attempt to constrain from the QSO-galaxy cross-correlation results.

4.2 A comparison of models and data

We calculate the expected clustering amplitude, $\omega(\theta < 120'')$, for a number of different cases which are shown in Table 3. We first use the known present day galaxy-galaxy auto-correlation function with $r_0 = 6 h^{-1}$ Mpc and $\gamma = 1.8$. With clustering evolution which is stable in comoving coordinates this model is inconsistent with the data for all $z < 1.5$ QSOs at the 3.5σ level. Clustering which is stable in proper coordinates is rejected at the 2.6σ level and clustering evolution which is consistent with linear theory is rejected at the 2.2σ level. If we allow for an integral constraint of ~ 0.006 , which of course assumes a clustering amplitude similar to the auto-correlation amplitude of $b_J < 23$ galaxies, the significance of the results are only changed by $\sim 0.3\sigma$. This correction would be considerably smaller if we used the measured cross-correlation amplitude to estimate an integral constraint. In fact the integral constraint would be negative, increasing the significance of the above rejections. Results from three other sets of parameters are also shown in

Table 3. Predicted clustering amplitudes, $\omega(\theta < 120'')$ and A_{qg} (assuming the given value of γ), for $z < 1.5$ QSOs and $b_J < 23$ galaxies in a number of different models. σ gives the significance of the difference between the models and the observed clustering for all QSOs with $z < 1.5$. No correction is made for the integral constraint.

r_0	γ	ϵ	$\omega(\theta < 120'')$	A_{qg}	σ
6.0	1.8	-1.2	0.0430	0.00170	3.5
6.0	1.8	0.0	0.0245	0.00099	2.6
6.0	1.8	0.8	0.0175	0.00071	2.2
14.0	1.8	-1.2	0.1976	0.00797	11.2
14.0	1.8	0.0	0.1128	0.00454	7.0
14.0	1.8	0.8	0.0805	0.00324	5.4
8.8	2.2	-1.2	0.3179	0.00233	17.2
8.8	2.2	0.0	0.1867	0.00136	10.7
8.8	2.2	0.8	0.1360	0.00100	8.2
2.0	1.8	-1.2	0.0060	0.00024	1.7
2.0	1.8	0.0	0.0034	0.00014	1.5
2.0	1.8	0.8	0.0024	0.00010	1.5

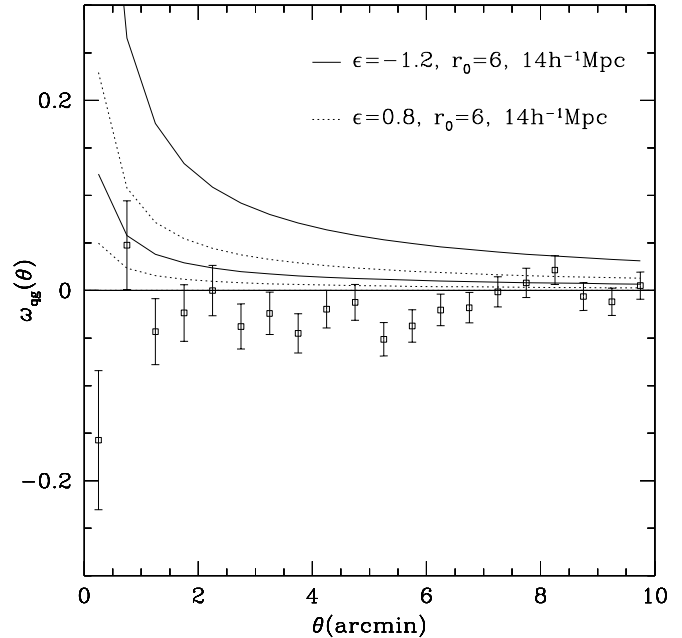


Figure 8. $\omega(\theta)$ calculated from the models discussed in the text compared to the results from all QSOs with $z < 1.5$ correlated with $b_J < 23$ galaxies. The solid curves show models with comoving clustering evolution ($\epsilon = -1.2$) and amplitudes of $r_0 = 14 h^{-1}$ Mpc (upper) and $6 h^{-1}$ Mpc (lower). The dotted curves show models with linear theory clustering evolution ($\epsilon = 0.8$) and amplitudes of $r_0 = 14 h^{-1}$ Mpc (upper) and $6 h^{-1}$ Mpc (lower).

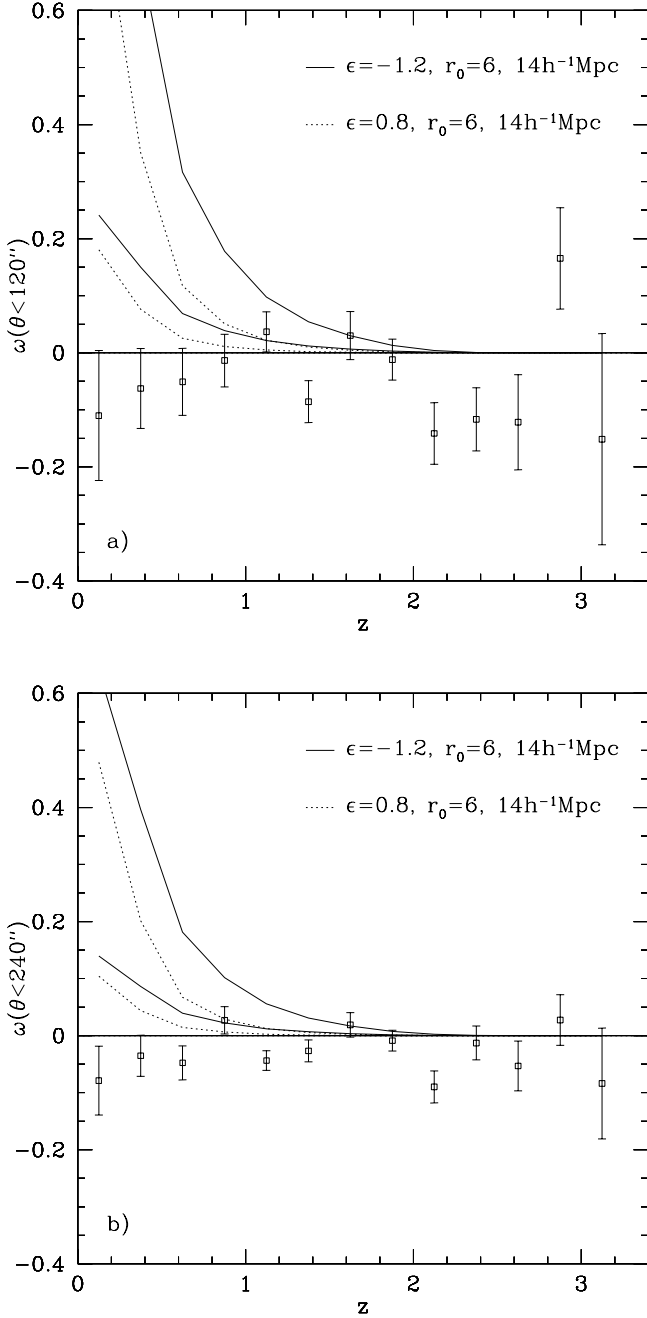


Figure 9. a) $\omega(\theta < 120'')$ and b) $\omega(\theta < 240'')$ calculated from the models discussed in the text compared to the results from all QSOs as a function of redshift. The solid curves show models with comoving clustering evolution ($\epsilon = -1.2$) and amplitudes of $r_0 = 14 h^{-1} \text{ Mpc}$ (upper) and $6 h^{-1} \text{ Mpc}$ (lower). The dotted curves show models with linear theory clustering evolution ($\epsilon = 0.8$) and amplitudes of $r_0 = 14 h^{-1} \text{ Mpc}$ (upper) and $6 h^{-1} \text{ Mpc}$ (lower).

Table 3. With a clustering amplitude similar to that of the cluster-cluster auto-correlation function $r_0 = 14 h^{-1} \text{ Mpc}$ and $\gamma = 1.8$ (Dalton et al. 1994), the lowest amplitude found (assuming linear theory growth) is 5σ too high compared with the data. We then try a model which fits the galaxy-cluster cross-correlation function, $r_0 = 8.8 h^{-1} \text{ Mpc}$ and $\gamma = 2.2$, (Lilje & Efstathiou 1988). This model, which might be a better estimate of our expected signal if QSOs were found only in rich clusters, is comfortably rejected for any reasonable rate of evolution. Finally we test a model with very low clustering amplitude, $r_0 = 2 h^{-1} \text{ Mpc}$, similar to that found in the Canada-France Redshift Survey (Le Fevre et al. 1996) for $I_{\text{AB}} < 22.5$ galaxies with a median redshift of 0.56. This is clearly a better fit to our results, being discrepant by only $\sim 1.5\sigma$. Ideally we would attempt to find the best fit values for r_0 and ϵ using maximum likelihood techniques. However, as the measured cross-clustering amplitude is marginally negative, these best fit values would have no physical meaning. Fig. 8 demonstrates that on scales $> 120''$ the data are also inconsistent with the models, out to $\sim 8'$. The cross-correlation is, on average, negative up to this scale and inclusion of an integral constraint of the magnitude discussed above (Section 2) has no significant effect on this statement.

The models are also plotted as a function of redshift in Fig. 9. Fig. 9a is for $\omega(\theta < 120'')$ while Fig. 9b is for $\omega(\theta < 240'')$. These first demonstrate the relative stability of using a $120''$ radius aperture to calculate the clustering amplitude. Secondly, they show the redshift at which the models can be rejected. In Fig. 9b, all the models plotted are inconsistent with the data for redshifts less than $z \sim 1.5$.

4.3 The effect of gravitational lensing

Our results suggest that there could be a lensing component to the cross-correlation of faint, $b_J < 23$, galaxies and optically selected QSOs, as a small anti-correlation was measured between the two populations. Similar anti-correlations between brighter galaxies and UVX QSO candidates have been interpreted in terms of gravitational lensing by Croom (1997). This anti-correlation is due to the two competing effects of magnification and area distortion. If the number-magnitude relation of the lensed objects is flat, there are only a small fraction of objects that are added to the sample through amplification, so that the area distortion wins, reducing the perceived number density.

Here we attempt to model the effect of the lensing contribution on this result. Using the redshift distributions of the galaxy and QSO populations we construct Monte-Carlo simulations to calculate the expected correlation signal as a function of redshift. These simulations model the individual galaxy potentials as isothermal spheres, and take into account the clustering of galaxies by also adding a constant density plane. Wu et al. (1996) calculate that the maximum matter surface density contributed by large-scale structure is $\sim 0.01 - 0.02 h \text{ g cm}^{-2}$ assuming that the amount of matter in galaxies is $\Omega_g \sim 1$. Typical velocity dispersions for galaxies are $\sim 200 \text{ km s}^{-1}$, so we produce Monte-Carlo simulations with velocity dispersions of 200 and 400 km s^{-1} and constant density planes with $\Sigma = 0.0$ and $0.02 h \text{ g cm}^{-2}$. We use a value of 0.28 for the slope of the QSO integral number-count slope. Fig. 10 shows how the clustering amplitude in

these simulations changes with redshift. The extreme case of $\Sigma = 0.02h \text{ g cm}^{-2}$ and $\sigma = 400 \text{ km s}^{-1}$, which can contribute ~ -0.02 to the correlation amplitude, can account for most of the negative signal found for QSOs at $z < 1.5$, while it cannot account for the negative correlation found at higher z . Fig. 10b shows the $\omega(\theta)$ predicted by the lensing models, for a combination of all the QSOs at $z < 1.5$, compared to the data. Correcting the data to allow for this lensing effect would not give the correlation function a positive amplitude. Lensing has no effect on the rejection of high clustering amplitude models, but does make the models with low clustering amplitude more consistent with the data.

5 DISCUSSION

It is clear that there is strong disagreement between the clustering results presented here and a range of models. This is demonstrated by Fig. 8. At $z < 1.5$ the correlation within $120''$ is $\omega(\theta < 120'') = -0.027 \pm 0.020$, and at $z > 1.5$, the combined X-ray and optically selected sample has a clustering amplitude of $\omega(\theta < 120'') = -0.028 \pm 0.021$, almost identical to that found at lower redshift. If we assume that a non-zero cross-correlation is only produced by physically associated QSOs and galaxies then the above results give us strong constraints on the environments of radio-quiet QSOs up to $z \sim 1 - 1.5$. Out to this redshift we still expect to see significant numbers of galaxies with a limiting magnitude of $b_J = 23$. The local luminosity function has $M_J^* \simeq -19.7$ (e.g. Ratcliffe 1996) which is equivalent to $b_J = 23$ and 24 for $z = 1.0$ and $z = 1.5$ without K-corrections. A combination of K-correction and reasonable luminosity evolution (Pozzetti et al. 1996) leaves these values largely unchanged (particularly for late type galaxies) and thus at $z = 1$ we reach $\sim M^*$ and at $z = 1.5$ about 1 mag brighter than M^* . We can firmly reject the hypothesis that the QSOs in our data exist in rich environments similar to galaxy clusters. This is true for a wide range of evolutionary rates (parameterized by ϵ). A scenario in which QSOs have poorer environments, similar to ‘normal’ galaxies, is a more acceptable alternative, although this still gives a clustering amplitude which is inconsistent with the data at the $2 - 3\sigma$ level.

We see a significant anti-correlation in our data, which cannot be explained by the conventional clustering models used above, but the data give us various clues as to the source of this signal. First, we find that the optically selected QSOs show more anti-correlation than the X-ray selected samples, particularly at high redshift. Secondly, when we sub-divide the galaxy samples on the basis of colour (for only two fields), we find that the red galaxies show a stronger anti-correlation than the blue galaxies. It has been established that the auto-correlation amplitude for faint red galaxies is significantly higher than for faint blue galaxies (Roche et al. 1996). This is easily understood if the redder galaxies lie predominantly at low redshift while the high redshift tail of the galaxy distribution is composed of the blue population. Of course, early type galaxies are also more numerous in rich structures such as galaxy clusters. It therefore appears that QSOs tend to show an anti-correlation with galaxies in rich environments at low redshift.

The possible causes of this signal are either obscuration by high densities of dust in rich structures or gravi-

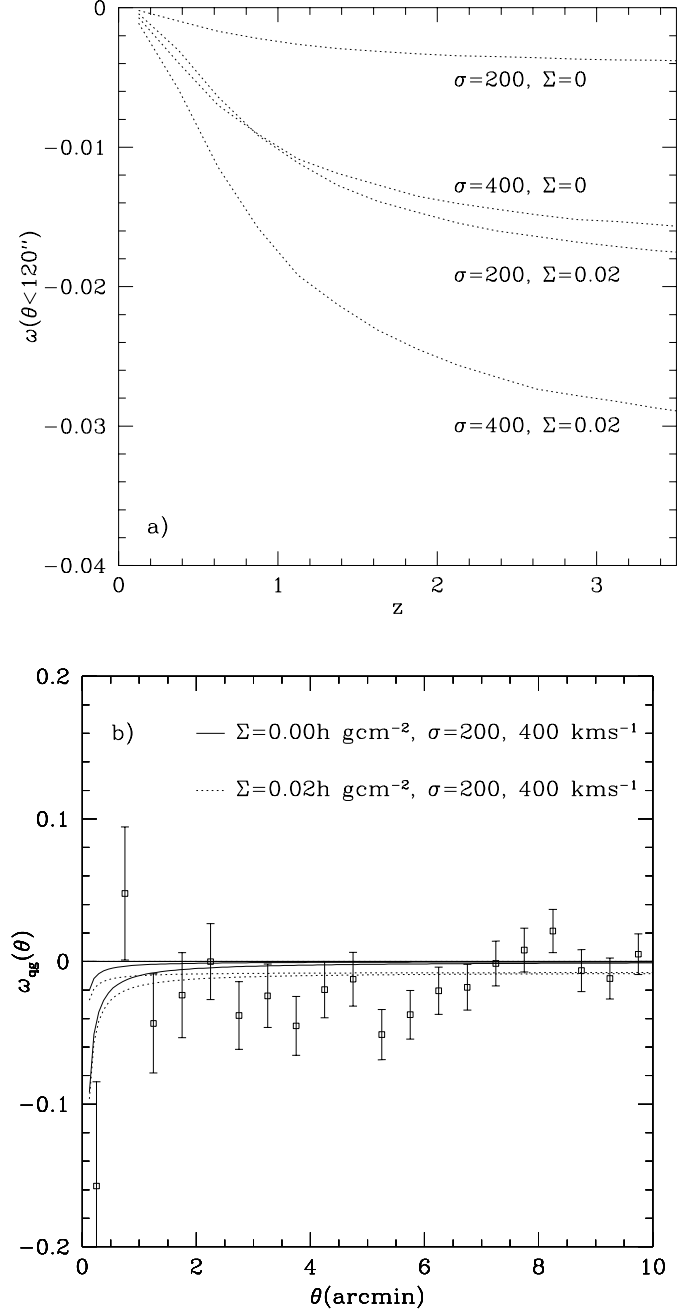


Figure 10. Estimated angular cross-correlation function of QSOs with faint, $b_J < 23$, galaxies due to lensing. a) $\omega(\theta < 120'')$ as a function of QSO redshift. The correlation amplitude is measured within $120''$ from Monte-Carlo simulations, with velocity dispersions 200 and 400 km s^{-1} and planes with $\Sigma = 0.0$ and $0.02h \text{ g cm}^{-2}$ mass surface densities. b) $\omega(\theta)$ for the four different lensing models for all QSOs with $z < 1.5$ compared to the measured $\omega(\theta)$.

tational lensing which can cause an anti-correlation if the QSO number-counts slope is flat (e.g. Narayan 1989). The optical QSOs in the sample are in the magnitude range where the number counts are flat, ~ 0.3 , compared to the critical slope of 0.4 which is the slope required for zero-correlation. The X-ray selected QSOs, in contrast, have a $\log N - \log S$ slope of 2.52 ± 0.3 at bright magnitudes turning over to 1.1 ± 0.9 (Georgantopoulos et al. 1996). The critical $\log N - \log S$ slope is 1.0 so we expect no anti-correlation (although it should be noted that the errors in the slope at faint fluxes are large). Above we show that even extreme estimates of galaxy masses could only produce anti-correlations of $\omega(\theta) \sim -0.02$ to -0.03 . This extreme model can just account for the anti-correlation measured. Lensing could reduce the inconsistency between our results and the lowest amplitude clustering models to only $\sim 1\sigma$, while the inconsistency with the strongly clustered models is still very significant. Lensing does not appear to explain the larger anti-correlation found at $z > 1.8$ between the $b_J < 23$ galaxies and optical QSOs, although it should be noted that this signal is due to a relatively small number of QSOs. A final possibility is that QSOs at low redshift might avoid rich environments. However, we have only a small number of QSOs at low redshift which are in fields that contain colour information (7 QSOs at $z < 1$), and also, other observations (Smith et al. 1995) find a low but positive correlation between QSOs and galaxies at low redshift.

Finally we note that deep wide field CCD imaging will allow this study to be developed further. Deep, $B < 26$, imaging in an area of ~ 2 sq. deg. will be presented in the second paper in this series (Croom & Shanks 1998 in preparation). This data will allow us to probe QSO environments at higher redshift $z \sim 2$, and determine if the present study may have missed small, faint galaxies associated with lower redshift QSOs.

6 CONCLUSIONS

We have carried out an investigation of the environments of a large sample of QSOs (~ 150), using deep AAT photographic plates in 5 independent areas. The QSOs were selected by both optical colour techniques and deep X-ray exposures from *ROSAT*. We draw the following conclusions:

1. Most QSOs show zero or negative correlations. For a combination of all QSOs at $z < 1.5$ we find $\omega(\theta < 120'') = -0.027 \pm 0.020$. Only a small number of QSOs ($\sim 4 - 5$) show significant positive correlation with $b_J \leq 23$ galaxies;

2. Optically and X-ray selected QSOs show marginally different properties, with the optical sample being more anti-correlated than the X-ray sample; for $z < 1.5$ the X-ray selected sample gives $\omega(\theta < 120'') = -0.018 \pm 0.022$, while the optically selected sample gives $\omega(\theta < 120'') = -0.051 \pm 0.027$. At high redshift, $z > 2$, the optical QSOs become more anti-correlated with galaxies.

3. Analysis of the two fields with colour information suggests that the anti-correlation is stronger in the red galaxy population than in the blue population.

4. The cross-correlation results are compared with models which include clustering evolution. Models which have clustering amplitudes similar to that of galaxy clusters ($r_0 \sim 14 h^{-1}$ Mpc) with a wide range of evolutionary rates are

ruled out. The data are more consistent with a low clustering amplitude, similar to that of the galaxy auto-correlation function, although $r_0 = 6 h^{-1}$ Mpc combined with linear theory evolution still gives too high an amplitude at the 2σ level. Models with $r_0 = 2 h^{-1}$ Mpc are only $\sim 1.5\sigma$ above the observed cross-correlation. If gravitational lensing causes some of the measured anti-correlation, the disagreement with the low amplitude clustering model could be reduced to $\sim 1\sigma$.

5. We suggest that the anti-correlation found could be due to gravitational lensing, particularly as the optical QSOs and red galaxies show the strongest anti-correlation. An extreme lensing model could account for most of the measured anti-correlation at $z < 1.5$. However, even this extreme lensing model does not significantly affect our conclusions when comparing the data to clustering models.

The results presented here clearly reject the notion that radio-quiet QSOs exist in rich cluster-like environments up to $z \sim 1 - 1.5$. Beyond this redshift we require deeper images to determine the environments of QSOs, these observations will be important in the interpretation of new QSO large-scale structure measurements from the next generation of QSO surveys (e.g. the 2dF QSO Redshift Survey, Smith et al. 1997).

Our results are consistent with those of Boyle & Couch (1993) who find no correlation between $R \sim 23$ galaxies and QSOs in the redshift range $0.9 < z < 1.5$. Ellingson et al., (1991) find a marginal positive signal at $z < 0.6$, which is consistent with our data (although we have a small number of QSOs at these low redshifts). Our data appear to be inconsistent with those of Hutchings et al., (1995) who find that a sample of 9 out of 14 QSOs are associated with compact groups of star forming galaxies, although these objects lie in a QSO *super-cluster* and so may be a unrepresentative sample existing in a particularly rich environment. We conclude that our results continue to uphold the hypothesis that QSOs are not strongly biased with respect to the galaxy population, but are more likely to trace the distribution of *normal* galaxies.

ACKNOWLEDGEMENTS

This paper was prepared using the facilities of the STAR-LINK node at the University of Durham. SMC acknowledges the support of a Durham University Research Studentship. We thank Robert Smith for many useful comments concerning this paper.

REFERENCES

- Almaini, O., 1996, PhD Thesis, University of Durham.
- Boyle, B. J. & Couch, W. J., 1993, MNRAS, 264, 604.
- Boyle, B. J., Fong, R., Shanks, T., & Peterson, B. A., 1990, MNRAS, 243, 1.
- Boyle, B. J., Jones, L. R., & Shanks, T., 1991, MNRAS, 251, 482.
- Bruzual, A. G. & Charlot, S., 1993, ApJ, 405, 538.
- Condon, J.J., Cotton, W.D., Greisen, W.E., Yin, Q.F., Perley, R.A., Taylor, G.B. & Broderick, J.J., 1998, AJ, 115, 1693.
- Cowie, L. L., Hu, E. M., & Songaila, A., 1995, Nature, 377, 603.
- Croom, S.M., 1997, PhD Thesis, University of Durham.

- Croom, S. M., Shanks, T., 1996, *MNRAS*, 281, 893.
- Dalton, G. B., Croft, R. A. C., Efstathiou, G., Sutherland, W. J., Maddox, S. J., & Davis, M., 1994, *MNRAS*, 271, L47.
- Ellingson, E., Yee, H. K. C., & Green, R. F., 1991, *ApJ*, 371, 49.
- Georgantopoulos, I., Stewart, G. C., Shanks, T., Boyle, B. J., & Griffiths, R. E., 1996, *MNRAS*, 280, 276.
- Gregory, P.C., Vavasour, J.D., Scott, W.K. and Condon, J.J., 1994, *ApJS*, 90, 173.
- Hintzen, P., Romanishin, W., & Valdes, F., 1991, *ApJ*, 366, 7.
- Hutchings, J. B., Crampton, D., & Johnson, A., 1995, *AJ*, 109, 73.
- Jones, L. R., Fong, R., Shanks, T., Ellis, R. S., & Peterson, B. A., 1991, *MNRAS*, 249, 481.
- Lilje, P. B. & Efstathiou, G., 1988, *MNRAS*, 231, 635.
- Le Fevre, O., Hudon, D., Lilly, S.J., Crampton, D., Hammer, F., Tresse, L., 1996, *ApJ*, 461, 534.
- Limber, D. N., 1953, *ApJ*, 117, 134.
- Maddox, S. J., Sutherland, W. J., Efstathiou, G., & Loveday, J., 1990, *MNRAS*, 243, 692.
- Metcalfe, N., Shanks, T., Campos, A., Fong, R., & Gardner, J. P., 1996, *Nature*, 383, 236.
- Narayan, R., 1989, *ApJ*, 339, L53.
- Peebles, P. J. E., 1980, *The Large-Scale Structure of the Universe*, Princeton.
- Pozzetti, L., Bruzual, G., & Zamorani, G., 1996, *MNRAS*, 281, 953.
- Ratcliffe, A., 1996, PhD Thesis, University of Durham.
- Roche, N., 1994, PhD Thesis, University of Durham.
- Roche, N., Shanks, T., Georgantopoulos, I., Stewart, G. C., Boyle, B. J., & Griffiths, R. E., 1995, *MNRAS*, 273, L15.
- Roche, N., Shanks, T., Metcalfe, N., & Fong, R., 1996, *MNRAS*, 280, 397.
- Smith R.J., 1998, PhD Thesis, University of Cambridge.
- Smith, R.J., Boyle, B.J., Shanks, T., Croom, S.M., Miller, L., Read, M., 1997, *Proc. IAU symp.* 179.
- Smith, R. J., Boyle, B. J., & Maddox, S. J., 1995, *MNRAS*, 277, 270.
- Shanks, T., Boyle, B. J., Griffiths, R. E., Stewart, G. C., Georgantopoulos, I., & Almaini, O., 1998, In preparation.
- Wu, X. P., Fang, L. Z., Zhu, Z. H., & Qin, B., 1996, *ApJ*, 471, 575.
- Yee, H. K. C. & Green, R. F., 1987, *ApJ*, 319, 28.
- Yee, H. K. C. & Green, R. F., 1984, *ApJ*, 280, 79.
- Zitelli, V., Mignoli, M., Zamorani, G., Marano, B., & Boyle, B. J., 1992, *MNRAS*, 260, 925.